ACS APPLIED ELECTRONIC MATERIALS

pubs.acs.org/acsaelm Article

All-Electrical Control and Temperature Dependence of the Spin and Valley Hall Effect in Monolayer WSe_2 Transistors

Xintong Li, Zhida Liu, Yihan Liu, Suyogya Karki, Xiaoqin Li, Deji Akinwande, and Jean Anne C. Incorvia*

Cite This: *ACS Appl. Electron. Mater.* 2022, 4, 3930−3937 Read Online

ACCESS | Metrics & More | Article Recommendations | Supporting Information

ABSTRACT: Heavy metal-based two-dimensional van der Waals materials have a large, coupled spin and valley Hall effect (SVHE) that has potential use in spintronics and valleytronics. Optical measurements of the SVHE have largely been performed below 30 K, and understanding of the SVHE-induced spin/valley polarizations that can be electrically generated is limited. Here, we study the SVHE in monolayer p-type tungsten diselenide (WSe_2). Kerr rotation (KR) measurements show the spatial distribution of the SVHE at different temperatures, its persistence up to 160 K, and that it can be electrically modulated via gate and drain bias. A spin/valley drift and diffusion model together with a reflection measurement and a four-port electrical measurement is used to interpret the KR data. A lower-bound spin/valley lifetime is predicted to be of 40 ns and a mean free path of 240 nm below 90 K, 2 orders of magnitude higher than a previous work that uses similar methods. The spin/valley polarization on the edge is calculated to be ∼4% at 45 K. These results are important steps toward practical use of the SVHE.

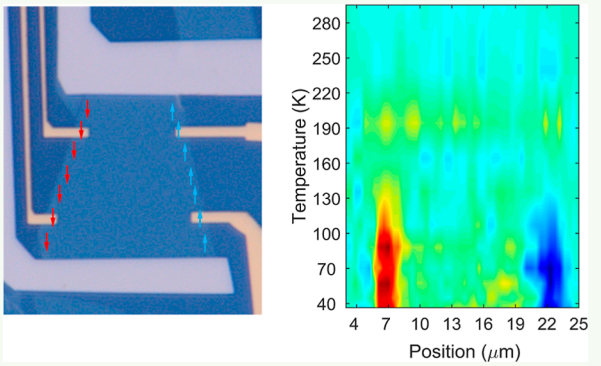

KEYWORDS: *spin and valley Hall effect, spatial Kerr rotation measurement, monolayer tungsten diselenide, spin/valley lifetime, mean free path*

INTRODUCTION

The spin and valley degrees of freedom in two-dimensional (2D) van der Waals materials and heterostructures provide platforms for novel physics and potential applications in spintronics and valleytronics.[1−7] Compared with graphene, transition-metal dichalcogenide monolayers possess an intrinsically broken inversion symmetry, together with strong spin−orbit coupling, which leads to a coupled spin and valley Hall effect (SVHE) that makes the electrical generation and manipulation of spin and valley polarizations convenient.[8−10] Monolayer tungsten diselenide (WSe_2) features a significant valence band spin-splitting (0.46 eV)[11] and a p-type behavior in field effect transistors (FETs), making it an ideal platform for electro-optical modulation of the spin and valley degrees of freedom.[12] The intervalley scattering of holes in WSe_2 must also flip spin, resulting in a prolonged spin and valley lifetime.[13] While all-electrical measurements of the spin or valley Hall effect have been performed at room temperature,[14−16] it is a challenge to distinguish the SVHE non-local electrical signal from other potential sources, including a variety of unclear effects that are unrelated to spin and valley, similar to those reported in previous works on graphene.[17−19] Optical measurements of electrically generated SVHE, on the other hand, can directly image the spatial distribution of the polarization and can be used to extract more parameters. Previous work has demonstrated, via spatial Kerr rotation (KR) measurements, the observation of the SVHE in n-type bilayer[20] and monolayer[21] MoS_2 and in p-type monolayer WSe_2 FETs[22] at temperatures from 20 to 30 K. However, little work has shown electrical control of the SVHE, and detailed interpretation of the SVHE-induced KR data and the study of the temperature and carrier density dependence of SVHE parameters are sorely lacking. Also, in a previous report that calculated the spin/valley lifetime, mean free path, and polarization, the high contact resistance of the device hindered the estimation and resulted in a very low estimation of these parameters.[22]

Here, we study the spatial distribution of the SVHE in monolayer WSe_2 FETs at different temperatures via spatial KR measurements and show its persistence up to 160 K. We show that the SVHE can be electrically modulated by gate and drain bias. By measuring the reflectance spectra versus temperature, voltage, and probing laser energy, a conversion is developed

Received: May 5, 2022
Accepted: July 20, 2022
Published: August 9, 2022

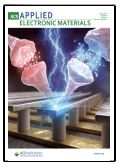

between the measured KR signal and spin/valley imbalance density. A four-port electrical measurement is conducted to exclude the effect of the contact resistance, and a more accurate four-port mobility and channel electric field is calculated. We then develop a spin/valley drift diffusion model to interpret the data and calculate the lower-bound of spin/valley lifetime and mean free path as well as estimate the spin/valley polarization on the edge of the channel. A more detailed comparison between this work and other work on the SVHE can be found in Supporting Information S1 to show the critical advancements made in the present work.

In the WSe_2 transistor, a hole current flows through the WSe_2 channel when applying a drain bias and a negative gate bias to the transistor, and a spin/valley current is generated in the transverse direction by the SVHE, which causes spin/valley accumulation on the two edges that can be optically observed using linearly polarized light. The SVHE is illustrated in Figure 1a. Magneto-optical Kerr effect (MOKE) measurement is

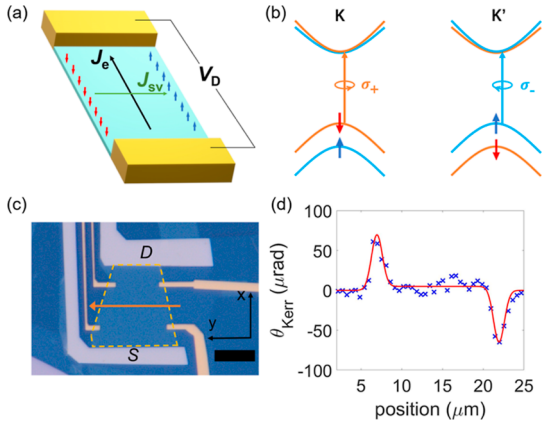

Figure 1. (a) Illustration of the device structure and SVHE. A source−drain voltage V_D is applied on the source and drain contacts (yellow), with source grounded, and a negative gate voltage V_G is applied to tune the doping level. A spin/valley current J_{sv} is generated by the SVHE, which is perpendicular to the charge current J_e. (b) Schematic of the spin and valley dependence of the optical selection rule for right- (σ_+) and left- (σ_-) handed polarized lights. Arrows with colors mark the spin-split conduction band minima and valance band maxima at K and K′ valleys. (c) Optical image of a typical WSe_2 FET device. The yellow dashed line marks the monolayer WSe_2 channel. The orange arrow marks the direction of the optical line scans. Drain (D) and source (S) contacts are marked. Other contacts are for four-port voltage measurements and are fabricated after the optical measurements. The black scale bar is 10 μm. (d) Typical spatial line scan of the KR measuring the SVHE with data (blue crosses) and the fitting curve (red line) that accounts for the width of the Gaussian laser beam.

conducted to measure the spin/valley polarization distribution along a transverse line, without applying external magnetic fields. Figure 1b shows the schematic of the spin−split conduction band minima and valence band maxima near the K and K′ valleys. The optical selection rule demands the absorption of circularly polarized light to be spin- and valley-dependent.[9,23] With incident linearly polarized light, a KR will occur in the reflected light if there is a local spin and valley imbalance in monolayer WSe_2 since the left- and right-circularly polarized components experience a different dielectric environment. Thus, the magnitude of the KR signal indicates spin/valley polarization, and the KR sign should be opposite for the two valleys due to the opposite sign of the Berry curvature around K and K′ valleys.

Figure 1c shows an optical image of one of the monolayer WSe_2 transistors. Images of more devices can be found in Supporting Information S2. Note that although the SiO_2 substrate and lack of encapsulation lower the sample quality, the presented structure is used since it provides a flat, bubble-free surface and it requires a lower laser power in the KR measurements than hexagonal boron nitride (hBN)-encapsulated samples, although the latter structure provides a better sample quality and mobility. We also fabricated devices with monolayer WSe_2 on hBN but found that the spatial KR measurement had additional noise most likely due to the random air bubbles between WSe_2 and hBN. These bubbles create local strain on the WSe_2 layer and non-uniform gating that disturbs the charge current and induces additional signals of KR angles locally. One of the typical spatial line scans of KR at 45 K is shown in Figure 1d with the line scan direction across the WSe_2 channel shown by the arrow in Figure 1c. Opposite-sign peaks in KR are observed on opposite edges of the WSe_2 channel, showing the SVHE. The red line is a fitting curve that will be described below.

EXPERIMENTAL SECTION

The devices are fabricated by the following process. Si wafers with 125 nm SiO_2 are cleaned by piranha solution and an ozone ultraviolet (UV) cleaner. Monolayer WSe_2 is obtained by mechanical exfoliation from a bulk WSe_2 to a PDMS stamp. The flake is then transferred to the Si/SiO_2 wafer right after the UV clean following a high vacuum annealed at 200 °C for 6 h. E-beam lithography (EBL) is conducted to define the contact area for the source and drain. Then, Pd (40 nm) is deposited in a high-vacuum e-beam evaporation tool with a base pressure of 2.5×10^{-8} Torr. Then, another EBL and metal deposition step is used to fabricate the 5 nm Cr/75 nm Au metal pads for following wire bonding. Additional EBL and thermal plasma etching steps are applied on some samples to define a better shape for the monolayer channel and to detach the device from WSe_2 multilayers. After the optical measurements, additional contacts are fabricated near the edge of the channel for four-port electrical measurements. The reason why these contacts are fabricated afterward is that they will disturb the optical measurements when the laser spot is close to the metal.

The reflection spectra are measured with an energy ranging from 660 nm (1.879 eV) to 780 nm (1.590 eV) using a white light source. The source and drain are grounded, and a VG up to ±26 V is applied. The spectra are measured with a spectrometer. The same spot of WSe_2 is used for the measurement, and the spectra on SiO_2 are also measured. During the measurement, no difference is observed when we move the laser spot to the middle or near the edges of the sample.

A spatial KR measurement of the SVHE-induced spin/valley polarization is conducted in a monolayer WSe_2 transistor. A DC V_G and an AC V_D are applied to the wire-bonded WSe_2 transistor in a cryostat, with an AC frequency of 520 Hz. This frequency ensures that the change of V_D is slow compared with the spin/valley lifetime, which is in the range of nanoseconds to microseconds, and it is also much larger than the resistor and capacitor time constant. A frequency ranging from 100 to 1500 Hz is used in the test, and no change in the KR is observed. Then, 520 Hz is used for better noise rejection. A linearly polarized continuous wave laser with a wavelength of 700.0 nm (1.7714 eV) is used to detect the KR. The laser is focused by an objective and impinges on the sample under normal incidence. The laser power is kept as low as 1.5 μW: it was found on additional devices that a larger laser power degraded the contacts and shifted the threshold gate voltage. The full width at half-maximum (fwhm) of the Gaussian laser beam was measured to be 1.57 μm by a line scan of the reflection across a metal edge on the sample and fitted with an error function. A half-wave plate and a Wollaston prism split the reflected

https://doi.org/10.1021/acsaelm.2c00599
ACS Appl. Electron. Mater. 2022, 4, 3930−3937

beam, and the split beams are detected by balanced photodetectors. The output voltage signal, which is proportional to the KR, is magnified and read by a lock-in amplifier that is locked to the frequency of V_D. This voltage is denoted as V_{Kerr}. The voltage signal V_{Kerr} is then converted to the KR angle by $\theta_{Kerr} = \frac{V_{Kerr}}{4\sqrt{2}\, V_{chopper}}$, where $V_{chopper}$ represents the voltage reading using a lock-in amplifier when using a chopper to measure the total light intensity in one of the detectors in the balanced photodetector (the other detector is blocked).

RESULTS AND DISCUSSION

Two-Port and Four-Port Electrical Test. Two-port DC electrical characterization of monolayer WSe_2 FETs is conducted at different temperatures, and four-port electrical measurements are conducted at room temperature (RT) after the optical measurements. Four-port and two-port source−drain conductance versus V_G characteristics, measured in an ambient environment at RT, are presented in Figure 2a, for V_D = 2 V. A four-port field-effect hole mobility of μ = 7.3 cm^2/(V s) is extracted from the curve at V_G = −22 V. This value is consistent with previous reports on similar samples and is smaller than the phonon-scattering limited mobility at RT.[24,25] Almost no n-type behavior is detected under a V_G up to +20 V. More electrical test results can be found in Supporting Information S3. Figure 2b shows the I_D versus V_D characteristic of the same device at RT with various V_G after intense KR measurement. The inset shows an I_D−V_D curve measured at 45 K. The shape of the curve at a low temperature indicates the existence of a Schottky barrier. Since the channel mobility should increase at lower temperatures in this range,[26] R_C becomes more dominant over the series resistance when cooling.

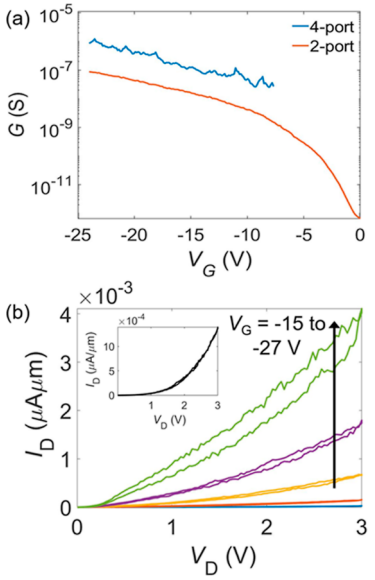

Figure 2. (a) Monolayer WSe_2 FET four-port and two-port conductance G vs V_G transfer characteristics measured in an ambient environment at RT. The four-port conductance is ∼10 times larger than the two-port conductance since the large contact resistance is excluded in the four-port measurement. A four-port mobility of μ = 7.3 cm^2/(V s) is extracted. (b) I_D vs V_D characteristic measured at RT with V_G = −15, −18, −21, −24, and −27 V after intense KR measurements. The inset shows an I_D−V_D curve measured at 45 K with V_G = −22 V. The shape of the curve at a low temperature indicates the existence of a Schottky barrier.

Gate Voltage- and Temperature-Dependent Reflection Spectra Measurement and Modeling. Gate voltage-dependent reflection spectra were measured on the monolayer WSe_2 transistor at selected temperatures with a white light source. Figure 3a shows a grayscale plot of the measured differential reflection spectra $\Delta R/R$ versus V_G at 45 K, where $\Delta R/R = (R_{WSe_2} - R_{SiO_2})/R_{SiO_2}$ is the relative change of reflection of monolayer WSe_2 (R_{WSe_2}) with respect to the reflection of the Si/SiO_2 background (R_{SiO_2}). The peak at ∼1.745 eV under a small V_G bias represents the absorption of neutral A exciton (X^0). When increasing (decreasing) V_G, a higher density of electrons (holes) is induced in the WSe_2 channel. X^0 tends to capture an additional electron (hole) and forms a negatively (positively) charged trion X^- (X^+) that has a smaller peak energy, shown by the reflection spectra peaks that appear at higher V_G magnitudes. The trion peaks are recently described in many body pictures as attractive polarons, but in here we still denote them as X^- and X^+. With increasing carrier density, the oscillator strength of X^0 decreases while that of the trions increases. A broadening of the line width of X^0 absorption is also observed with increasing carrier density. More data can be found in Supporting Information S4. We use a similar method from previous works[22,27] to fit these data and extrapolate the relation between the complex reflectivity and the carrier density of monolayer WSe_2. The complex dielectric function dispersion $\varepsilon(E) = \varepsilon_1(E) + i\varepsilon_2(E)$ is modeled as a superposition of Lorentzian oscillators

$$\varepsilon(E) = 1 + \sum_k \frac{f_k}{E_k^2 - E^2 - iE\gamma_k} \quad (1)$$

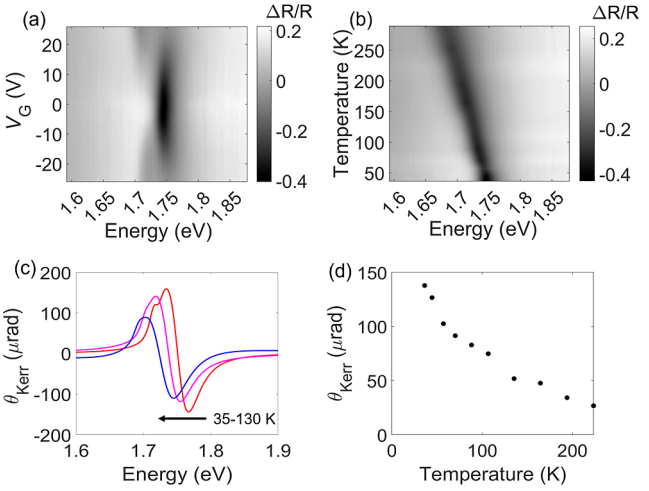

Figure 3. (a) Measured 2D grayscale plot of the differential reflection spectra $\Delta R/R$ vs V_G at 45 K. The peak at ∼1.745 eV under a small V_G bias shows the neutral A exciton (X^0). With increasing (decreasing) V_G, the X^0 peak gets weaker, while the X^- (X^+) peak with a smaller energy appears. (b) Measured differential reflection spectra $\Delta R/R$ as a function of temperature with V_G = 0 V. The X^0 peak red-shifts from 1.745 eV at 45 K to 1.681 eV at 290 K. (c) Modeled expected KR angle with an assumed spin/valley density imbalance of 1×10^{10} cm^{-2} as a function of photon energy at 35, 85, and 130 K. (d) Modeled expected KR plotted against temperature for a photon energy of 1.745 eV and an assumed spin/valley density imbalance of 1×10^{10} cm^{-2}.

https://doi.org/10.1021/acsaelm.2c00599
ACS Appl. Electron. Mater. 2022, 4, 3930−3937

Here, f_k, E_k, and γ_k are the oscillator strength, resonant energy, and linewidth of the kth oscillator. In this treatment, instead of having E_k run over the entire spectra, we only fit the oscillators corresponding to X^0 and X^- (X^+) and write the rest of the terms as a constant ε_b. Using the standard transfer matrix analysis on thin-film stacks,[28] the first derivative of the $\Delta R/R$ spectra is fit with the modeled function under measured V_G and temperature. The WSe_2 monolayer is treated as a homogeneous medium with a thickness of 6.49 Å. Details of the modeling can be found in Supporting Information S5. Since the total hole density p can be calculated from V_G by $p = C_G(V_G - V_T)$, where C_G is the gate oxide capacitance per unit area and V_T is the gate voltage at the charge neutral point, we obtained a relationship between $\varepsilon(E)$ and the total hole density p at different temperatures.

The $\varepsilon(E)$ versus p relationship is used to predict how much KR angle (θ_{Kerr}) can be generated from a given spin/valley sheet density imbalance Δp_{sv}, when a linearly polarized light impinges on the WSe_2 sample under normal incidence. Details can be found in Supporting Information S6. For example, it is found that $\frac{\Delta p_{sv}}{\Delta \theta_{Kerr}} = 7.3 \times 10^7$ cm^{-2}/μrad for small Δp_{sv} under a V_G of −22 V at 45 K, when probing with a 700 nm (1.771 eV) laser, which is close to the higher-energy side of X^0. This means that for a laser focused on an infinitesimal area of WSe_2, each μrad of measured KR corresponds to a spin/valley sheet density imbalance of 7.3×10^7 cm^{-2} at that area. This value is consistent with previous work.[22] We argue that the $\frac{\Delta p_{sv}}{\Delta \theta_{Kerr}}$ value is carrier density-dependent (and therefore V_G-dependent) and should not be ignored in KR analysis. Figure S6 in the Supporting Information shows this modeled dependence by plotting the predicted KR angle with a spin/valley density imbalance of 1×10^{10} cm^{-2} as a function of V_G, when probing with a 700 nm laser. This number 1×10^{10} cm^{-2} is chosen as a typical value that yields a KR that is close to the measured value.

The measured $\Delta R/R$ spectra as a function of temperature are shown in Figure 3b with $V_G = 0$ V. The X^0 peak red-shifts gradually from 1.745 eV at 45 K to 1.681 eV at 290 K as the absorption peak gets broadened. The same modeling, as above, is conducted for every temperature measured. In Figure 3c, the modeled expected KR angle with a spin/valley density imbalance of 1×10^{10} cm^{-2} at $V_G = -22$ V is plotted as a function of photon energy for a range of temperatures. Figure 3d shows the expected KR probed by a 700 nm laser versus temperature. Due to the red shift and broadening of the absorption peaks, the expected KR decreases with increasing temperature if a laser with a wavelength of 700 nm is used. This effect must be carefully calibrated in temperature-dependent spin/valley polarization calculations. More details will be discussed in the following section.

Low-Temperature KR Measurement and Modeling Shows Electrical Modulation of SVHE. KR measurement of the SVHE-induced spin/valley polarization is performed in the monolayer WSe_2 transistor shown in Figure 1c. No meaningful KR was detected on the SiO_2 background. Figure 4a,b shows the KR scanned along a line across the WSe_2 channel (direction depicted in Figure 1c) as a function of V_D and V_G, with fixed V_G and V_D, respectively. The width of the WSe_2 channel is 16 μm along this line. The marks are experimental data, and the curves are fits considering the finite fwhm of the Gaussian laser beam (details described below). The maximum

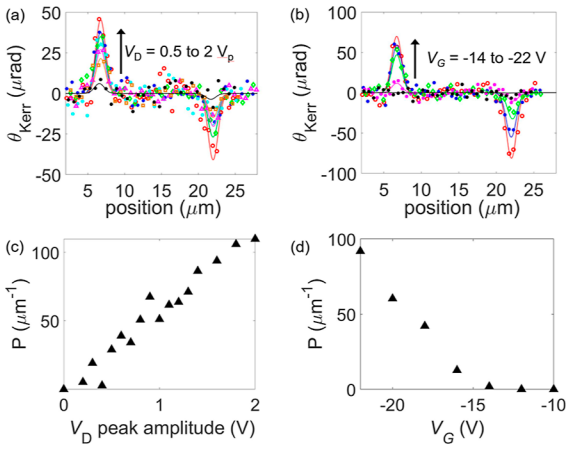

Figure 4. (a) Measured KR angle scanned along a transverse line on the WSe_2 channel as a function of V_D at 100 K. The V_D peak voltages are chosen to be 0.5, 0.8, 1.1, 1.4, 1.6, 1.8, and 2.0 V, while V_G is held constant at −22 V. (b) KR angle scanned across the WSe_2 channel as a function of V_G at 45 K. V_G = −14 to −22 V with an interval of −2 V and V_D is held to a constant AC amplitude of 2 V_p. For (A,B), the markers represent measured data, and the lines are fitted curves considering the fwhm of the laser. (c) Integrated spin/valley imbalance per unit length along the edge P, converted from the measured KR at the fixed spot on the edge where the KR is maximum, as a function of peak V_D. (d) P as a function of V_G. Note that the KR appears at V_G = −15 V.

of V_G and peak V_D are limited to −22 V and 2 V_p, respectively, to protect the device during measurement. We observe clear KR only on the WSe_2 edges, with opposite signs at opposite edges. Note that a small overall negative KR offset across the sample is subtracted from the data. Examples of original data can be found in Supporting Information S7. The offset is due to the magnetoelectric effect induced by the strain in the channel[21] and the drain voltage modulation of the carrier density in the channel, where an overall reflection modulation that is not fully canceled at the balanced photodetectors brings a finite KR reading. Offsets from these origins are expected to be uniform in the transverse direction and are much smaller than the measured peak-to-peak KR at the two edges. Also, the carrier density imbalance induced by these sources is negligible compared with the gate-induced total carrier density. Thus, we conclude that the subtraction of the offset is reasonable. The consistency of the measured data and the fitted profile of the Gaussian laser beam indicate that the spin/valley accumulation at the edges spans only a small distance toward the middle. This shows that the SVHE can be controlled purely electrically for device applications.

We then use a spin/valley drift-diffusion model and recall the analysis in previous reflection measurements to interpret the measured KR at 45 K. In the steady state, the spin/valley Hall current density J_{sv} in the transverse direction is balanced by the spin/valley relaxation at the edges

$$J_{sv} = \frac{e p_0 l_d}{\tau_{sv}} \tag{2}$$

where e is the elementary charge, p_0 is the spin/valley density imbalance at the edges, l_d is the diffusion length, and τ_{sv} is the spin/valley lifetime. Note that in the case of hole doping, we did not treat the spin Hall and valley Hall effects differently like what has been done in a previous work, where the spin Hall effects for electrons in n-doped MoS_2 are neglected due to the

https://doi.org/10.1021/acsaelm.2c00599
ACS Appl. Electron. Mater. 2022, 4, 3930−3937

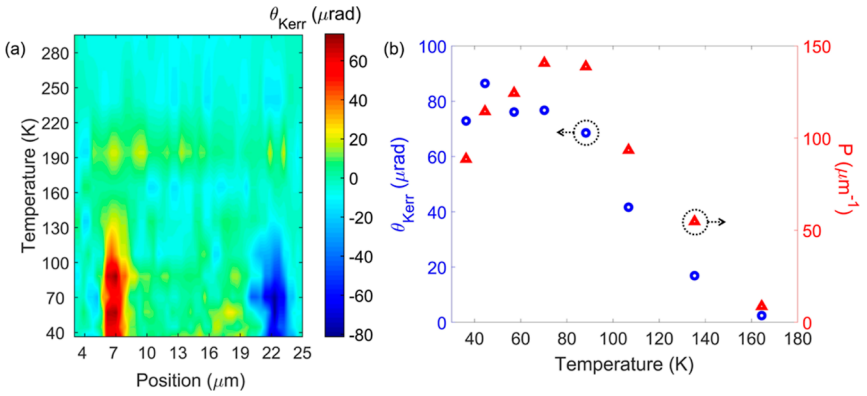

Figure 5. (a) KR spatial line scan as a function of temperature. Color represents magnitude of KR in μrad. The KR peaks become undetectable above 160 K because the spin/valley polarization drops drastically, and the KR is buried in noise. (b) Measured average KR of the two peaks (blue circles) and corresponding calculated spin/valley imbalance per unit length P (red triangles) vs temperature.

small spin splitting in the conduction band.[20] In p-doped WSe_2, due to its large spin-splitting in the valence band, both the spin Hall and valley Hall effects contribute greatly to the effective magnetization that generates the KR. Therefore, in the following treatment, we consider the spin and valley coupled ("spin/valley"). The spin/valley sheet density distribution along the transverse (y) direction can be modeled by

$$p_{sv}(y) = p_0(e^{-\frac{y}{l_d}} - e^{y-w/l_d}) \quad (3)$$

Here, w is the channel width. In the measurements shown in Figure 4a,b, we see that the KR is due to the spin/valley imbalance that is highly concentrated near the edge and l_d cannot be detected directly by the spatial scan with finite laser fwhm, which suggests that $l_d \ll$ fwhm. We can use eq 3 and the Gaussian distribution of the light intensity to convert the measured peak KR at the edges to $P \equiv p_0 l_d$, which is the integral of $p_{sv}(y)$ along the y direction for either edge. Recall that in Figures S6 and 3d, we provided a way to calculate the spin/valley sheet density imbalance Δp_{sv} from the measured KR θ_{Kerr} and plotted the V_G and temperature dependence of $\frac{\Delta p_{sv}}{\Delta \theta_{Kerr}}$. Then, the integral P can be calculated by

$$P = \sqrt{\frac{\pi}{4 \ln 2}}\,\mathrm{fwhm}\frac{\Delta p_{sv}}{\Delta \theta_{Kerr}}\theta_{Kerr} \quad (4)$$

under the condition of $l_d \ll$ fwhm, where θ_{Kerr} is the KR angle measured directly in the MOKE test, while $\frac{\Delta p_{sv}}{\Delta \theta_{Kerr}}$ is the multiplier calculated from the reflection test.

Combining the definition of $P \equiv p_0 l_d$ with eq 2

$$P = \frac{\tau_{sv} J_{sv}}{e} = \frac{\tau_{sv}\sigma_{sv}}{e}E_x \quad (5)$$

Here, σ_{sv} is the spin/valley conductivity and E_x is the electric field in the charge current direction (x). The actual E_x of the WSe_2 channel can be estimated by $E_x = V_{ch}/L$, where V_{ch} is the voltage drop of the channel and L is the channel length. Due to the large contact resistance, two-port measurements highly overestimate V_{ch} and E_x. Our four-port measurements, on the other hand, can measure V_{ch} more accurately, without the effect of contact resistance. Since the four-port measurement is conducted only at RT, V_{ch} and E_x at low temperatures are still slightly overestimated because it is known that the channel conductance decreases due to the increase of mobility when lowering the temperature, while the contact resistance increases. P converted from measured KR at a fixed spot on the edge as a function of peak V_D and V_G, measured at 45 K, is shown in Figure 4c,d.

For the plot of P versus V_D at 45 K shown in Figure 4c, ideally there should be a linear relationship since τ_{sv} and σ_{sv} depend little on V_D bias, and E_x is proportional to V_D as shown in a previous work.[21] The Schottky barrier, however, should break the linear relationship between E_x and V_D, especially at a small bias, and make the $P-V_D$ curve more like the I_D-V_D curve shown in the Figure 2b inset. The observed near-linear $P-V_D$ at a small bias curve may arise from the low signal-to-noise ratio of the KR at a low bias. We found that P = 109 μm^{-1} at V_D = 2 V and V_G = −22 V.

The linearity between P and V_D can be used to estimate the lower bound of the spin (valley) lifetime τ_{sv}. The σ_{sv} is predicted to be proportional to the hole density in the valence band when the doping level is small. Here, we use the number from a first principle study[29] of the intrinsic spin Hall conductivity, $\sigma_{sv} = 2.2 \times 10^{-4} \times 10^2/\hbar$ for the carrier density in the device. There are extrinsic contributions to the Hall conductivity as well, including skew scattering and side-jump. In our experiment, skew scattering is negligible since it only dominates in the ultra-clean limit. Although the side-jump Hall conductivity cannot be easily distinguished from the intrinsic spin Hall conductivity, a previous work[30] shows that they have opposite signs and are similar in magnitude in WSe_2. Thus, it is reasonable to use the intrinsic spin Hall conductivity to estimate the lifetime. With these parameters, the lower bound of the spin/valley lifetime is estimated to be 34 ns at 45 K. This value agrees very well with previous time-resolved KR measurements[13,31,32] on similar WSe_2 samples, indicating that the calculation above is reasonable. Since the spin/valley mean free path l_d cannot be directly measured due to the limitation of the spatial resolution of the laser scan, $l_d = \sqrt{D\tau_{sv}}$ can be used to estimate it. The diffusion coefficient D can be calculated from the mobility calculated during the low-temperature electrical measurement. $l_d \approx$ 150 nm is calculated at 45 K, which agrees well with a previous work;[16] then, $p_0 = P/l_d$ is used to estimate the spin/valley density imbalance at the edge to be 7.3×10^{10} cm^{-2}. Gate voltage V_G at the charge neutral point is estimated to be equal to the charge current threshold voltage $V_T = 10 \pm 3$ V; then, the total hole density p

https://doi.org/10.1021/acsaelm.2c00599
ACS Appl. Electron. Mater. 2022, 4, 3930−3937

$= C_{ox}(V_G - V_T) = (1.73 \pm 0.52) \times 10^{12}$ cm^{-2}. Thus, the spin/valley polarization on the edge is approximately 4%.

The V_G dependence of P at $V_D = 2$ V$_p$ shown in Figure 4d is more complicated to interpret quantitatively. The linear relationship between σ_{sv} and hole density is the dominant effect, which also explains the fact that the V_G at which KR starts to turn on is close to V_T. The non-linearity between P and V_G is mainly due to the effect of τ_{sv}, where τ_{sv} was reported to be negatively correlated to the carrier density, but the dependence is relatively weak.[33]

Temperature Dependence of the SVHE. We now study the evolution of the SVHE KR signal with increasing temperature. Figure 5a shows the KR spatial line scan as a function of temperature, probed by a 700 nm laser. The KR peaks shows opposite signs at opposite edges at all temperatures below 160 K. To our knowledge, this is the highest temperature to date that the electrically induced SVHE has been measured optically, which shows a clear evidence of spin/valley accumulation at the edge.

In the left axis of Figure 5b, the average KR of the two peaks is plotted as a function of temperature, while on the right, the measured KR is converted to the excess spin/valley number per unit length, P, accounting for the extraneous effects described throughout the text. We fully accounted for the X^0 peak red shift and broadening when increasing the temperature. We found that during cooling, P appears at 160 K and grows fast until 90 K, where it starts to level and then decrease. For relatively high temperatures, τ_{sv} is dominated by phonon-assisted intervalley scattering[31] and drops fast with increasing temperature, while σ_{sv} is reported to have a relatively weak temperature dependence,[34] resulting in a fast decrease of P from 90 to 160 K. For a temperature below 90 K, we attribute the degradation of P when lowering the temperature to the weaker temperature dependence of τ_{sv} combined with decreasing channel E_x. It was shown in previous works that the intervalley scattering at low temperatures is no longer dominated by phonon-assisted scattering but is probably from scattering at grain boundaries and atomically sharp deformations,[35,36] resulting in a weaker temperature dependence of τ_{sv}. The temperature dependence of E_x is explained in Supporting Information S8. For temperatures higher than 160 K, τ_{sv} and P drop to a small value, and the resulting KR is buried in noise. We then roughly estimate τ_{sv} as a function of temperature by neglecting the weak temperature dependence of σ_{sv} and using the same method as that of the 45 K data, and the maximum $\tau_{sv} \approx 40$ ns is found at 90 K and a $\tau_{sv} \approx 2$ ns at 160 K is estimated. The mean free path l_d is calculated to be 240 nm at 90 K, and the corresponding polarization is 3%. The slightly higher τ_{sv} and l_d at 90 K than at 45 K is because these numbers at 45 K are more underestimated. Note that the condition $l_d \ll$ fwhm of the laser spot is met at all temperatures, consistent with the profile of the spatial KR scan. Also, we argue that it is possible to directly measure the spin/valley mean free path on p-doped WSe_2 with high mobility and lifetime using the spatial KR measurement since l_d can reach a few microns in these samples. To observe the SVHE at higher temperatures above 160 K, higher signal to noise is required.

CONCLUSIONS

We investigated the SVHE in monolayer WSe_2 transistors by measuring the spatial distribution of the KR induced by the spin and valley imbalance. The KR data were converted to the excess spin and valley per unit length along the edge, P, by carefully fitting the reflection spectra at different temperatures and doping levels with a sum of the Lorentzian oscillator of X^0 and X^+. It was found that P depends near-linearly on V_D or V_G bias and decreases with increasing temperature above 90 K. These results are explained using a spin/valley drift and diffusion model and a four-port electrical test to exclude the effect of the contact resistance. For example, at 45 K, $P = 109$ μm^{-1} was measured, and a polarization of 4% on the edge was calculated. The spin/valley lifetime of 40 ns is found at 90 K, and the corresponding mean free path is 240 nm, and the polarization on the edge is 3%. This lifetime and mean free path are 2 orders of magnitude higher than those of previous reports on the SVHE of WSe_2, and the lifetime is in good agreement with a previous time-resolved KR work, indicating that our modeling is reasonable. We conclude that the manipulation of spin and valley degrees of freedom by the SVHE at a higher temperature is possible. Our findings demonstrate the potential of monolayer WSe_2 devices as a platform for electrically generated spin and valley polarization at different temperatures.

ASSOCIATED CONTENT

Supporting Information

The Supporting Information is available free of charge at https://pubs.acs.org/doi/10.1021/acsaelm.2c00599.

Recent work on the SVHE in a few-layer TMD, images of more devices, electrical measurements, additional reflection spectra, modeling of the reflection spectra, converting the KR angle to spin/valley accumulation P, raw data for KR measurements, and temperature dependence of the channel electric field E_x (PDF)

AUTHOR INFORMATION

Corresponding Author

Jean Anne C. Incorvia − *Department of Electrical and Computer Engineering, The University of Texas at Austin, Austin, Texas 78712, United States;* orcid.org/0000-0002-4805-2112; Email: incorvia@austin.utexas.edu

Authors

Xintong Li − *Department of Electrical and Computer Engineering, The University of Texas at Austin, Austin, Texas 78712, United States;* orcid.org/0000-0001-8566-0558

Zhida Liu − *Department of Physics and Center for Dynamics and Control of Materials, The University of Texas at Austin, Austin, Texas 78712, United States*

Yihan Liu − *Department of Electrical and Computer Engineering, The University of Texas at Austin, Austin, Texas 78712, United States;* Present Address: Department of Electrical and Computer Engineering, University of Pittsburgh, Pennsylvania 15261, United States; orcid.org/0000-0001-9687-4914

Suyogya Karki − *Department of Electrical and Computer Engineering, The University of Texas at Austin, Austin, Texas 78712, United States;* orcid.org/0000-0002-5786-0410

Xiaoqin Li − *Department of Physics and Center for Dynamics and Control of Materials, The University of Texas at Austin, Austin, Texas 78712, United States*

Deji Akinwande − *Department of Electrical and Computer Engineering, The University of Texas at Austin, Austin, Texas 78712, United States;* orcid.org/0000-0001-7133-5586

Complete contact information is available at:

https://pubs.acs.org/10.1021/acsaelm.2c00599

Author Contributions

The manuscript was written through contributions of all authors. All authors have given approval to the final version of the manuscript. X.L. fabricated the devices, carried out the measurements, and wrote the manuscript. Z.L. and Y.L. assisted with the measurements. S.K. contributed to the measurement setup. X.-Q.L. supervised and contributed to the measurement setup. D.A. supervised. J.A.I. conceived of the project, led supervising of the work, and wrote the manuscript.

Funding

This research was primarily supported by the National Science Foundation (NSF) through the Center for Dynamics and Control of Materials: an NSF MRSEC under Cooperative Agreement No. DMR-1720595. The optical measurement setup was supported in part by the NSF-Major Research Instrumentation Program (Grant MRI-2019130). D.A acknowledges the Temple Foundation Endowed Professorship. Z. L. and X. L acknowledge the support from National Science Foundation (ECCS-2130552). This work was performed in part at the University of Texas Microelectronics Research Center, a member of the National Nanotechnology Coordinated Infrastructure (NNCI), which is supported by the National Science Foundation (Grant ECCS-2025227). The authors acknowledge the use of shared research facilities supported in part by the Texas Materials Institute and the Texas Nanofabrication Facility supported by NSF Grant No. NNCI-1542159.

Notes

The authors declare no competing financial interest.

■ ACKNOWLEDGMENTS

We would like to thank Bin Fang and Tsun Chun Chang for their guidance on the optical setup.

■ REFERENCES

(1) Rycerz, A.; Tworzydło, J.; Beenakker, C. W. J. Valley filter and valley valve in graphene. *Nat. Phys.* **2007**, *3*, 172−175.
(2) Vitale, S. A.; Nezich, D.; Varghese, J. O.; Kim, P.; Gedik, N.; Jarillo-Herrero, P.; Xiao, D.; Rothschild, M. Valleytronics: Opportunities, Challenges, and Paths Forward. *Small* **2018**, *14*, 1870172.
(3) Mak, K. F.; McGill, K. L.; Park, J.; McEuen, P. L. The valley hall effect in MoS_2 transistors. *Science* **2014**, *344*, 1489−1492.
(4) Tombros, N.; Jozsa, C.; Popinciuc, M.; Jonkman, H. T.; van Wees, B. J. Electronic spin transport and spin precession in single graphene layers at room temperature. *Nature* **2007**, *448*, 571−574.
(5) Han, W.; Kawakami, R. K.; Gmitra, M.; Fabian, J. Graphene spintronics. *Nat. Nanotechnol.* **2014**, *9*, 794−807.
(6) Drögeler, M.; Franzen, C.; Volmer, F.; Pohlmann, T.; Banszerus, L.; Wolter, M.; Watanabe, K.; Taniguchi, T.; Stampfer, C.; Beschoten, B. Spin Lifetimes Exceeding 12 ns in Graphene Nonlocal Spin Valve Devices. *Nano Lett.* **2016**, *16*, 3533−3539.
(7) Shimazaki, Y.; Yamamoto, M.; Borzenets, I. V.; Watanabe, K.; Taniguchi, T.; Tarucha, S. Generation and detection of pure valley current by electrically induced Berry curvature in bilayer graphene. *Nat. Phys.* **2015**, *11*, 1032−1036.
(8) Xiao, D.; Liu, G. B.; Feng, W.; Xu, X.; Yao, W. Coupled spin and valley physics in monolayers of MoS_2 and other group-VI dichalcogenides. *Phys. Rev. Lett.* **2012**, *108*, 196802.
(9) Mak, K. F.; He, K.; Shan, J.; Heinz, T. F. Control of valley polarization in monolayer MoS_2 by optical helicity. *Nat. Nanotechnol.* **2012**, *7*, 494−498.
(10) Komider, K.; González, J. W.; Fernández-Rossier, J. Large spin splitting in the conduction band of transition metal dichalcogenide monolayers. *Phys. Rev. B: Condens. Matter Mater. Phys.* **2013**, *88*, 245436.
(11) Zhu, Z. Y.; Cheng, Y. C.; Schwingenschlögl, U. Giant spin-orbit-induced spin splitting in two-dimensional transition-metal dichalcogenide semiconductors. *Phys. Rev. B: Condens. Matter Mater. Phys.* **2011**, *84*, 153402.
(12) Zhou, B. T.; Taguchi, K.; Kawaguchi, Y.; Tanaka, Y.; Law, K. T. Spin-orbit coupling induced valley Hall effects in transition-metal dichalcogenides. *Commun. Phys.* **2019**, *2*, 26.
(13) Dey, P.; Yang, L.; Robert, C.; Wang, G.; Urbaszek, B.; Marie, X.; Crooker, S. A. Gate-Controlled Spin-Valley Locking of Resident Carriers in WSe_2 Monolayers. *Phys. Rev. Lett.* **2017**, *119*, 137401.
(14) Hung, T. Y. T.; Rustagi, A.; Zhang, S.; Upadhyaya, P.; Chen, Z. Experimental observation of coupled valley and spin Hall effect in p-doped WSe_2 devices. *InfoMat* **2020**, *2*, 968−974.
(15) Safeer, C. K.; Ingla-Aynés, J.; Herling, F.; Garcia, J. H.; Vila, M.; Ontoso, N.; Calvo, M. R.; Roche, S.; Hueso, L. E.; Casanova, F. Room-temperature spin hall effect in Graphene/MoS_2 van der Waals heterostructures. *Nano Lett.* **2019**, *19*, 1074−1082.
(16) Wu, Z.; Zhou, B. T.; Cai, X.; Cheung, P.; Liu, G. B.; Huang, M.; Lin, J.; Han, T.; An, L.; Wang, Y.; Xu, S.; Long, G.; Cheng, C.; Law, K. T.; Zhang, F.; Wang, N. Intrinsic valley Hall transport in atomically thin MoS_2. *Nat. Commun.* **2019**, *10*, 1−8.
(17) Wang, Y.; Cai, X.; Reutt-Robey, J.; Fuhrer, M. S. Neutral-current Hall effects in disordered graphene. *Phys. Rev. B: Condens. Matter Mater. Phys.* **2015**, *92*, No. 161411(R).
(18) Cresti, A.; Nikolíc, B. K.; Garćia, J. H.; Roche, S. Charge, spin and valley Hall effects in disordered graphene. *Riv. Nuovo Cimento* **2016**, *39*, 587−667.
(19) Van Tuan, D.; Marmolejo-Tejada, J. M.; Waintal, X.; Nikolić, B. K.; Valenzuela, S. O.; Roche, S. Spin Hall Effect and Origins of Nonlocal Resistance in Adatom-Decorated Graphene. *Phys. Rev. Lett.* **2016**, *117*, 176602.
(20) Lee, J.; Mak, K. F.; Shan, J. Electrical control of the valley Hall effect in bilayer MoS_2 transistors. *Nat. Nanotechnol.* **2016**, *11*, 421−425.
(21) Lee, J.; Wang, Z.; Xie, H.; Mak, K. F.; Shan, J. Valley magnetoelectricity in single-layer MoS_2. *Nat. Mater.* **2017**, *16*, 887−891.
(22) Barré, E.; Incorvia, J. A. C.; Kim, S. H.; McClellan, C. J.; Pop, E.; Wong, H. S. P.; Heinz, T. F. Spatial Separation of Carrier Spin by the Valley Hall Effect in Monolayer WSe_2 Transistors. *Nano Lett.* **2019**, *19*, 770−774.
(23) Yao, W.; Xiao, D.; Niu, Q. Valley-dependent optoelectronics from inversion symmetry breaking. *Phys. Rev. B: Condens. Matter Mater. Phys.* **2008**, *77*, 235406.
(24) Podzorov, V.; Gershenson, M. E.; Kloc, C.; Zeis, R.; Bucher, E. High-mobility field-effect transistors based on transition metal dichalcogenides. *Appl. Phys. Lett.* **2004**, *84*, 3301−3303.
(25) Chuang, H. J.; Tan, X.; Ghimire, N. J.; Perera, M. M.; Chamlagain, B.; Cheng, M. M. C.; Yan, J.; Mandrus, D.; Tománek, D.; Zhou, Z. High mobility WSe_2 p - And n - Field-effect transistors contacted by highly doped graphene for low-resistance contacts. *Nano Lett.* **2014**, *14*, 3594−3601.
(26) Movva, H. C. P.; Rai, A.; Kang, S.; Kim, K.; Fallahazad, B.; Taniguchi, T.; Watanabe, K.; Tutuc, E.; Banerjee, S. K. High-Mobility Holes in Dual-Gated WSe_2 Field-Effect Transistors. *ACS Nano* **2015**, *9*, 10402−10410.
(27) Li, Y.; Chernikov, A.; Zhang, X.; Rigosi, A.; Hill, H. M.; Van Der Zande, A. M.; Chenet, D. A.; Shih, E. M.; Hone, J.; Heinz, T. F. Measurement of the optical dielectric function of monolayer transition-metal dichalcogenides: MoS_2, $MoSe_2$, WS_2, and WSe_2. *Phys. Rev. B: Condens. Matter Mater. Phys.* **2014**, *90*, 205422.
(28) Byrnes, S. J. Multilayer Optical Calculations, **2016**; Vol. *1*−*20*, arXiv:1603.02720 [physics.comp-ph].
(29) Feng, W.; Yao, Y.; Zhu, W.; Zhou, J.; Yao, W.; Xiao, D. Intrinsic spin Hall effect in monolayers of group-VI dichalcogenides: A first-principles study. *Phys. Rev. B: Condens. Matter Mater. Phys.* **2012**, *86*, 165108.

(30) Shan, W. Y.; Lu, H. Z.; Xiao, D. Spin Hall effect in spin-valley coupled monolayers of transition metal dichalcogenides. *Phys. Rev. B: Condens. Matter Mater. Phys.* **2013**, *88*, 125301.
(31) Song, X.; Xie, S.; Kang, K.; Park, J.; Sih, V. Long-Lived Hole Spin/Valley Polarization Probed by Kerr Rotation in Monolayer WSe_2. *Nano Lett.* **2016**, *16*, 5010−5014.
(32) Kim, J.; Jin, C.; Chen, B.; Cai, H.; Zhao, T.; Lee, P.; Kahn, S.; Watanabe, K.; Taniguchi, T.; Tongay, S.; Crommie, M. F.; Wang, F. Observation of ultralong valley lifetime in WSe_2/MoS_2 heterostructures. *Sci. Adv.* **2017**, *3*, No. e1700518.
(33) Ersfeld, M.; Volmer, F.; Rathmann, L.; Kotewitz, L.; Heithoff, M.; Lohmann, M.; Yang, B.; Watanabe, K.; Taniguchi, T.; Bartels, L.; Shi, J.; Stampfer, C.; Beschoten, B. Unveiling Valley Lifetimes of Free Charge Carriers in Monolayer WSe_2. *Nano Lett.* **2020**, *20*, 3147−3154.
(34) Krstajić, P. M.; Vasilopoulos, P.; Tahir, M. Spin- and valley-polarized transport in a monolayer of MoS_2. *Phys. Rev. B* **2016**, *94*, No. 041419(R).
(35) Zeng, H.; Dai, J.; Yao, W.; Xiao, D.; Cui, X. Valley polarization in MoS2 monolayers by optical pumping. *Nat. Nanotechnol.* **2012**, *7*, 490−493.
(36) Hsu, W. T.; Chen, Y. L.; Chen, C. H.; Chen, P. S.; Liu, T. H.; Hou, L. J.; Li, W. H.; Chang, W. H. Optically initialized robust valley-polarized holes in monolayer WSe_2. *Nat. Commun.* **2015**, *6*, 8963.

https://doi.org/10.1021/acsaelm.2c00599
ACS Appl. Electron. Mater. 2022, 4, 3930−3937